

Investigating the clinical aspects of using CT vs. CT-MRI images during organ delineation and treatment planning in prostate cancer radiotherapy

Athanasis Tzikas¹, Pantelis Karaikos^{2,3}, Nikos Papanikolaou⁴, Panagiotis Sandilos^{2,5}, Efi Koutsouveli², Eleftherios Lavdas⁶, Christos Scarleas², Konstantinos Dardoufas^{2,5}, Bengt K. Lind¹, Panayiotis Mavroidis^{1,7}

¹Department of Medical Radiation Physics, Karolinska Institutet and Stockholm University, Sweden

²Department of Radiotherapy and Medical Physics, Hygeia Hospital, Athens, Greece

³Department of Medical Physics, Medical School, University of Athens, Athens, Greece

⁴Department of Radiological Sciences, University of Texas Health Science Center, San Antonio, Texas, USA

⁵Department of Radiology, Areteion University Hospital, Athens, Greece

⁶Department of Radiology, Larissa University Hospital, Larissa, Greece

⁷Department of Medical Physics, Larissa University Hospital, Larissa, Greece

Abstract

Background and purpose: In order to apply highly conformal dose distributions, which are characterized by steep dose fall-offs, it is necessary to know the exact tumor location and extension. This study aims at evaluating the impact of using combined CT-MRI images in organ delineation compared to using CT images alone, on the clinical results.

Materials and methods: For 10 prostate cancer patients, the respective CT and MRI images at treatment position were acquired. The CTV, bladder and rectum were delineated using the CT and MRI images, separately. Based on the CT and MRI images, two CTVs were produced for each patient. The mutual information algorithm was used in the fusion of the two image sets. In this way, the structures drawn on the MRI images were transferred to the CT images in order to produce the treatment plans. For each set of structures of each patient, IMRT and 3D-CRT treatment plans were produced. The individual treatment plans were compared using the biologically effective uniform dose (\bar{D}) and the complication-free tumor control probability (P_+) concepts together with the DVHs of the targets and organs at risk and common dosimetric criteria.

Results: For the IMRT treatment, at the optimum dose level of the average CT and CT-MRI delineated CTV dose distributions, the P_+ values are 74.7% in both cases for a \bar{D}_{CTV} of 91.5 Gy and 92.1 Gy, respectively. The respective average total control probabilities, P_B are 90.0% and 90.2%, whereas the corresponding average total complication probabilities, P_I are 15.3% and 15.4%. Similarly, for the 3D-CRT treatment, the average P_+ values are 42.5% and 46.7%, respectively for a \bar{D}_{CTV} of 86.4 Gy and 86.7 Gy, respectively. The respective average P_B values are 80.0% and 80.6%, whereas the corresponding average P_I values are 37.4% and 33.8%, respectively. For both radiation modalities, the improvement mainly stems from the better sparing of rectum. According to these results, the expected clinical effectiveness of IMRT can be increased by a maximum ΔP_+ of around 13.2%, whereas of 3D-CRT by about 15.8% when combined CT-MRI delineation is performed instead of using CT images alone.

Conclusions: It is apparent that in both IMRT and 3D-CRT radiation modalities, the better knowledge of the CTV extension improved the produced dose distribution. It is shown that the CTV is irradiated more effectively, while the complication probabilities of bladder and rectum, which is the principal organs at risk, are lower in the CT-MRI based treatment plans.

*Corresponding author. Address: Panayiotis Mavroidis, Department of Medical Radiation Physics, Karolinska Institutet and Stockholm University, PO Box 260, S-171 76 Stockholm, Sweden. Tel: +46 8-5177 2225, Fax: +46 8-343525, E-mail address: panayiotis.mavroidis@ki.se

Introduction

Radiotherapy planning for prostate carcinoma has traditionally been performed on computed tomography (CT)-images, on which both the high dose areas (prostate with or without seminal vesicles) as well as the low dose areas (surrounding structures, such as the rectum and bladder) are anatomically delineated. However, magnetic resonance imaging (MRI) provides much more information than CT since it can superbly demonstrate the internal prostatic anatomy, prostatic margins and the extent of prostatic tumors [1-3]. Furthermore, addition of MRI to CT in consensus reading with a radiologist results in a moderate decrease of the CTV, but an important decrease of the inter-observer delineation variation, especially at the prostatic apex [4].

CT-derived prostate volumes are larger than MR derived volumes, especially toward the seminal vesicles and the apex of the prostate. Using MRI for delineation of the prostate reduces the amount of irradiated rectal wall, and could reduce rectal and urological complications [5]. More specifically, Debois and colleagues concluded that the additional use of axial and coronal MR scans, in designing the treatment plan for localized prostate carcinoma, improves substantially the localization accuracy of the prostatic apex and the anterior aspect of the rectum, resulting in a better coverage of the prostate and a potential to reduce the volume of the rectum irradiated to a high dose [6].

The location of the organs-at-risk (OAR) and their tolerance doses constitute a major factor that determines the prescribed dose in radiation treatment planning. OARs are usually located in the immediate vicinity of the clinical target volume (CTV). This characteristic often limits the dose that can be delivered to the tumor [7]. The Intensity Modulated Radiotherapy (IMRT) generates more conformal distributions as compared to techniques related to conventional and simple conformal radiation therapy. This characteristic leads to the reduction of the radiation dose and toxicity to nearby organs thus, significantly improving dose delivery in cancer therapy [8]. Presently, IMRT can be implemented by several treatment planning systems. However, it is a crucial and challenging process to properly evaluate and select the best treatment plan since the employed optimization methodology affects the final optimized treatment plans that are proposed.

There are many tools available that are used to evaluate a radiotherapy treatment plan, such as isodose distribution charts, dose volume histograms (DVH), maximum, minimum and mean doses of the dose distributions as well as DVH point dose constraints. All the already mentioned evaluation tools are based on dose only without taking into account the radiobiological parameters of tumors or OARs. It has been demonstrated that although competing treatment plans might have similar mean, maximum or minimum doses they may have significantly different radiobiological outcomes [9].

For complementing the evaluation and comparison of treatment plans, the biologically effective uniform dose ($\bar{\bar{D}}$) and complication-free tumor control probability (P_+) can be used [8,10]. The biologically effective uniform dose ($\bar{\bar{D}}$) denotes that any two dose distributions within a tumor or OAR are equivalent if they produce the same probability for tumor control or normal tissue complication, respectively [9]. In our study, the $\bar{\bar{D}}$ is formulated by taking into consideration the fact that effective doses averaged over both dose distribution and organ radiosensitivity are more relevant to the clinical outcome.

The purpose of this study was to determine the influence of CT vs. fused CT-MRI based prostate delineation on the dose to the target and organs at risk during external beam radiotherapy. Furthermore, we aimed at estimating the clinical effect of this factor by comparing treatment plans of different conformality and quality of imaging information using radiobiological measures. Ten representative cases of prostate cancer have been used in order to perform the evaluation of the treatment plans, which were produced using fused CT-MRI images and CT images alone, using conventional conformal and IMRT radiation modalities. The value of biological and physical factors that are associated with the effectiveness of the treatment plans has been validated by performing a simultaneous physical and biological evaluation. The implemented radiobiological procedure calculates the probability to accomplish complication-free tumor control taking into account the dose-response relations of the involved tumors and OARs [11-15].

Materials and methods

In this study, computed tomography (CT) and magnetic resonance imaging (MRI) images were acquired for 10 patients with localized prostate adenocarcinoma, in the position of treatment. All the patients were required to have a full bladder and were scanned in supine position with a knee support. The patients were scanned on a Siemens Somaton – Plus CT Scanner with 4 mm slice thickness. In the MRI examination, the patients were scanned immediately after the CT scanning under identical conditions (full bladder in supine position with the knee support and using a similar with the CT table top). A series of 40 axial, 30 sagittal and 30 coronal T2-weighted images (4 mm slice thickness) were acquired using a turbo spin echo, 3D sequence. In our hospital, CT–MR fusion is a routine procedure for target and structure delineation in prostate cancer patients. CT images were loaded as primary images and were used for dose calculations. MR images were loaded as secondary images and then fused with the corresponding CT images. The registration was performed using the mutual information algorithm of the Masterplan (Nucletron) radiotherapy treatment planning system.

The Clinical Target Volume (CTV), which includes the prostate gland and the seminal vesicles, was delineated using the CT and MRI images, separately. The CTV drawn on the MRI images was transferred to the CT images. The PTV was produced by adding to the CTV 1.0 cm margin in all directions apart from that towards rectum, which was 0.6 cm. So, for each patient 2 CTVs and 2 PTVs were produced based on the CT and MRI images, separately. The bladder and rectum were delineated in the CT images. Two four-field (box) 3D conformal plans using 18 MV and two IMRT treatment plans using 6 MV MLC fields were developed for each patient based on the different tissue delineations. The DVHs of the targets and organs at risk were calculated along with other common dosimetric criteria. The individual treatment plans were compared using the biologically effective uniform dose (\bar{D}) together with the complication-free tumor control probability (P_+).

Treatment modalities and planning criteria

For each patient, two 3-dimensional conventional conformal (CRT) and two MLC-based IMRT treatment plans were performed, based on the two different CTVs and PTVs generated and corresponded to the two different imaging modalities (CT and MR). CRT plans were performed using 18 MV and box technique. Multileaf collimators (MLCs) were conformally shaped using the beam's-eye view projections of the PTV plus a uniform margin of 0.6 cm to account for beam penumbra. For IMRT plans a seven-field configuration (gantry angles: 210°, 260°, 310°, 0°, 50°, 100°, and 150°) and 6-MV were used. The prescription dose was 76 Gy in 38 fractions with the 98% of the CTV covered by this prescription dose and the 95% of the PTV covered by the 95% of the prescription dose. Constraints for rectum were set such that no more than 35% and 17% of the rectum received more than 40 and 65 Gy, respectively and for bladder no more than 20% of the bladder received more than 70 Gy. A step-and-shoot approach with a total of approximately 70 multileaf collimator-shaped (MLC-shaped) fields was used for all patients. For all plans, the final dose calculation was performed using the single pencil beam algorithm and a 2 mm calculation grid.

Radiobiological treatment plan evaluation

The calculation of the response probabilities (expected treatment outcome) of the CTV and OARs was performed by applying the Poisson model [16,17]:

$$P(D) = \exp\left(-e^{e\gamma - (D/D_{50})(e\gamma - \ln(\ln(2)))}\right) \quad (1)$$

where $P(D)$ is the probability to control the tumor or induce a certain injury to a normal tissue that is irradiated uniformly with a dose D . D_{50} is the dose, which gives a 50% response and γ is the maximum normalized dose-response gradient. Parameters D_{50} and γ are specific for every organ and type of clinical endpoint. Before the application of Eq. (1), the dose distributions have to be corrected for the fractionation effects, which means that the knowledge of the α/β ratio is necessary [14,15,18,19].

Tumors are assumed to have a parallel structural organization since the eradication of all of the clonogenic cells is required. Taking this assumption into account the overall probability of tumor control P_B (B denotes benefit from tumor control), is given by the expression:

$$P_B(\vec{D}) = \prod_{i=1}^M P(D_i)^{\Delta v_i} \quad (2)$$

where M is the number of voxels or subvolumes in the tumor and Δv_i is the volume of each of those voxels or subvolumes. The probability $P(D_i)$ is calculated by Eq. (1).

Among the models that have been developed for calculating the response of normal tissues, the relative seriality model was chosen [17,19]. The relative seriality model is a model that accounts for the volume effect and for a heterogeneous dose distribution, the overall probability of injury P_I (I denotes injury) for a number of OARs is expressed as follows:

$$P_I = 1 - \prod_{j=1}^{N_{\text{organs}}} (1 - P_I^j) = 1 - \prod_{j=1}^{N_{\text{organs}}} \left(1 - [1 - \prod_{i=1}^{M_j} (1 - P^j(D_i)^{s_j})^{\Delta v_i}]^{1/s_j} \right) \quad (3)$$

where P_I^j is the probability of injuring organ j and N_{organs} is the total number of vital OARs. $P^j(D_i)$ is the probability of response of the organ j having the reference volume and being irradiated to dose D_i as described by Eq. (1). $\Delta v_i = \Delta V_i / V_{\text{ref}}$ is the fractional sub-volume of the organ that is irradiated compared to the reference volume for which the values of D_{50} and γ have been calculated. M_j is the total number of voxels or sub-volumes in the organ, and s_j is the relative seriality parameter that characterizes the internal organization of the organ. The dose-response parameters of the organs used in this study are based on published data and they are shown in Table 1 [12-15,18]. The uncertainties that are associated with these parameters are of the order of 5% for D_{50} , 30% for γ and 60% for s .

The concepts of P_+ and \bar{D} were used in this study to evaluate the effectiveness of the different treatment plans. P_+ expresses the probability of achieving tumor control without causing severe damage to normal tissues [10]. The probability of getting benefit from a treatment (tumor control) is denoted by P_B , whereas the probability for causing severe injury to normal tissues by P_I [8,19]. Using these quantities, P_+ can be estimated from the following expression:

$$P_+ = P_B - P_{B \cap I} = P_B - P_I \quad (4)$$

\bar{D} is the biologically effective uniform dose, which is the dose that causes the same tumor control or normal tissue complication probability as the actual dose distribution given to a certain tissue [8,9]. In this study, \bar{D} is derived from the following expression:

$$P_B(\vec{D}) \equiv P_B(\bar{D}_B) \quad (5)$$

where \vec{D} denotes the 3-dimensional dose distribution. By normalizing plans to a common prescription point (\bar{D}) and then plotting out the tissue response probability vs. \bar{D} curves, a number of plan trials can be compared based on radiobiological endpoints.

In this work, the treatment plans were evaluated radiobiologically by incorporating in the analysis the radiation sensitivities of the involved target and OARs. However, conventional physical criteria like dose volume histograms, isodose charts, etc, were also employed. The objective was to estimate the tumor control and normal tissue tolerance against the optimum target dose needed [20,21]. We used an internal developed ad-hoc software application in order to calculate the dose volume histograms (DVHs), the probabilities of injury and benefit, the complication-free tumor control probability (P_+) and the biologically effective uniform dose \bar{D} .

3. Results

We have used the physical and radiobiological characteristics in order to assess the effectiveness of the two radiation modalities and organ delineation approaches. Figs. 1 and 2 depict comparisons of the isodose curve distributions for the two modalities explored. The isodose line distributions are presented both in transverse and coronal planes in order to show better the association of the dose distribution

with the calculated DVHs. The comparison of the treatment plans in terms of DVHs and dose-response curves for the cancer type of prostate is shown in Figs. 3-5, respectively. More specifically, in the upper diagrams of the figures, the DVHs (Fig. 3), individual dose-response curves (Fig. 4) and $P_+ - \bar{\bar{D}}_B$ plots (Fig. 5) of the CT and CT-MRI based treatment plans are presented for the CRT (left) and IMRT (right) radiation modalities, respectively. The analytical results of these comparisons are presented in Tables 2 and 3. Nevertheless, since treatment plan development and optimization is usually performed using the CT images alone, we performed a second set of comparisons by transferring the CTV and OAR delineations based on the fused CT-MRI images to the treatment plans, which were developed based on the CT images alone in order to estimate the deviation that should be expected in the treatment outcome from this source of error. These comparisons of the CT and CT-MRI delineations based on the CT-based treatment plans are illustrated schematically in the lower diagrams of Figs. 3-5 and quantitatively in Tables 4 and 5 for the CRT (left) and IMRT (right) radiation modalities, respectively.

The individual dose-response curves of the CTV and each OAR are presented together with the P_+ curve. In the diagrams of Fig. 4, the response curves are all normalized to the mean dose in the CTV (\bar{D}_{CTV}). In the diagrams of Fig. 5, the dose-response curves have been normalized to the $\bar{\bar{D}}_B$, which forces the response curves of the CTV (P_B) of the different treatment plans to coincide. In these diagrams the same dose distribution is kept at all dose levels and the curves show how tissue responses change with dose prescription. The normalization using $\bar{\bar{D}}_B$ allows the inter-comparison of the different modalities on the same basis and gives emphasis to the therapeutic window, which characterizes each treatment plan. In Tables 2-5, a quantitative summary of the physical and biological comparisons is presented.

Figs. 1 and 2 illustrate the CRT and MLC-based IMRT dose distributions in the form of isodose curves according to which it appears that the MLC-based IMRT plan produces slightly higher inhomogeneity inside the CTV as compared to the 3D-CRT but otherwise very similar dose spread outside the CTV. The 3D-CRT radiation modality delivers higher mean doses to the GTV, lymph nodes and bladder as compared to the MLC-based IMRT. However, the MLC-based IMRT delivers a lower dose to the rectum.

For the treatment plans of the CRT treatment modality, which were produced based on the CT images, at the clinical dose prescription, the average P_+ value is 15.9% for a mean dose to the CTV, \bar{D}_{CTV} and $\bar{\bar{D}}_B = 75.5$ Gy. The average total control probability, P_B is 26.5% and the average total complication probability, P_I is 10.5%. Similarly, for the treatment plans that were produced based on the fused CT-MRI images, the average P_+ value is larger by 1.6% for the same \bar{D}_{CTV} and $\bar{\bar{D}}_B$. The average P_B is the same with that of the treatment plans that were produced using CT images alone and the average P_I is lower by 1.6%. However, if we optimize the dose level of the dose distributions in order to maximize the complication-free tumor control then for the CT-based treatment plans, the P_+ value becomes 42.5% for a $\bar{\bar{D}}_B$ of 86.4 Gy having average $P_B = 80.0\%$ and average $P_I = 37.4\%$.

Similarly, for the CT-MRI-based treatment plans, the P_+ value becomes 4.2% higher for a \bar{D}_B of 86.1 Gy having a higher average P_B by 0.6% and a lower average P_I by 3.6%.

For the treatment plans of the IMRT treatment modality, which were produced based on the CT images, at the clinical dose prescription, the P_+ value is 52.5% for $\bar{D}_{CTV} = 81.0$ Gy and $\bar{D}_B = 80.8$ Gy. The average P_B is 57.1% and the average P_I is 4.7%. Similarly, for the CT-MRI-based treatment plans, the P_+ value becomes 0.9% higher for $\bar{D}_{CTV} = 80.8$ Gy and $\bar{D}_B = 80.5$ Gy. The average P_B is higher by 1.5% and the average P_I is higher by 0.5%. However, if we optimize the dose level of the dose distributions in order to maximize the complication-free tumor control then for the CT-based plans, the P_+ value becomes 74.7% for a \bar{D}_B of 91.5Gy having $P_B = 90.0\%$ and $P_I = 15.3\%$. Respectively, for the CT-MRI-based plans, the P_+ value remains the same for a higher \bar{D}_B by 0.6 Gy. The corresponding average P_B is higher by 0.2%, whereas the average P_I is also higher by 0.1%.

If the CT-based treatment plans were applied to calculate the dose in target and organs delineations based on the fused CT-MRI images then the average differences would be almost zero in the case of CRT radiation modality (Table 4). On the contrary, in the case of IMRT radiation modality, the plans based on CT-MRI fused images are superior. The P_+ value would become 2.1% lower for a lower \bar{D}_{CTV} by 0.3 Gy and \bar{D}_B by 0.4 Gy. The average P_B would be lower by 2.1% while the average P_I would remain the same. At the dose level where the value of P_+ get maximum the differences become lower with the P_+ value being lower by 0.4% for a lower \bar{D}_B by 0.4 Gy. The average P_B would be lower by 0.5% and the average P_I would be lower by 0.2%, respectively.

A more quantitative description of the treatment plans is presented in Fig. 5. It is shown that both CRT and MLC-based IMRT are characterized by very conformal dose distributions, which deliver high doses to the CTV while sparing very well the OARs involved. At the prescribed dose level of the distributions, the mean doses to the CTV are high but not very close to the optimum level, which would maximize their therapeutic window (complication-free tumor control).

Discussion

Many studies have indicated that prostate volumes on CT are consistently larger than MR volumes [22,23]. This has as a consequence that the dose delivered to the rectal wall and bulb of the penis be significantly reduced in the treatment plans based on the MRI-delineated prostate compared with the CT-delineated prostate, allowing a dose escalation of 2.0-7.0 Gy for the same rectal wall dose [24]. In the present study, the volume of the CTV was 58.6 ± 18.8 cm³ when delineated on the CT images and 46.1 ± 17.8 cm³ when delineated on the fused CT-MRI images.

The acquisition sequence that was used in the MRI examination, was selected on the grounds that it depicts the pathology better than CT. MRI is generally characterized by a higher contrast resolutions than CT. Consequently, the pathology can be better distinguished from healthy tissue. In

this sense, the exact extension of the pathology within the prostate gland can be seen and delineated as well as the borders between the pathology and the surrounding healthy tissues.

In the majority of cases, the mean and maximum-minimum doses, the isodose distributions and the DVHs are inspected in order to evaluate the fitness of a treatment plan. Nevertheless, this information does not take into consideration the biological characteristics of the targets. The present study involves the application of both physical and radiobiological measures on ten prostate cancer cases that lead to the evaluation of the effectiveness of CRT and IMRT radiation modalities in relation to the use of fused CT-MRI and CT alone images in treatment planning. The physical analysis was performed using the dose distributions and the DVHs of the treatment plans. In order to evaluate and classify the different treatment plans we took into consideration the uniformity of the dose distribution in the target volume and the dose constraints to the OARs.

The CTV dose is less homogeneous in the MLC-based IMRT plan ($CV = 0.7\%$) as compared to the CRT ($CV = 0.5\%$) (Tables 2 and 3). As it is shown in Fig. 5, the expected complication-free tumor control for the CRT treatment plan is worse than the MLC-based IMRT for prescribed doses between 70-100 Gy. The reason for this is that the MLC-based IMRT irradiates more effectively the CTV with better sparing of the rectum as shown in Tables 2 and 3. In CRT, the significantly higher risk of rectal complications stem not only from the higher mean dose that is delivered to the rectum but also from the respectively higher maximum dose, which is related to the probability of inducing rectal complications due to the high relative seriality value of rectum.

The differences observed on the DVH comparisons between the CRT and MLC-based IMRT treatment plans are not always reflected in the radiobiological evaluation using the dose-response relations of the tissues involved. This is because the way a certain dose distribution affects an organ depends on its radiobiological characteristics. For example, although two dose distributions may have the same mean dose and standard deviation they may have different response probabilities when irradiating the same tissue. The advantages of the \bar{D} concept and its differences from other reporting means that have been reported in the literature are based on the fact that a 3-dimensional dose distribution may be reduced to a single dose, yielding the same response probability.

Due to the fact that different plans generally deliver different mean doses to the CTV for the same control rate, the use of the mean dose to the CTV as a dose scaling basis is not suitable since the expected response rates induced by the treatment to the rest of the involved organs cannot be easily compared using this scale (Fig. 4). In the diagrams of Fig. 5, where the \bar{D}_B is used, it is shown that the curves corresponding to the response of the CTV (P_B) coincide. When plotted in this way, the response curves of the organs at risk point out the treatment plan that is superior. Just as the dose volume histogram chart is a good illustration of the volumetric dose distribution delivered to the patient, so is the biological evaluation plot as a measure of the expected clinical outcome. The dose-response diagrams in conjunction with the dosimetric diagrams provide a more thorough viewpoint of the examined treatment plans.

Observing the diagrams in Fig. 5 it is apparent that the clinically established dose prescription, which corresponds to a certain uniform dose in the CTV deviates from the optimal dose level that the radiobiological evaluation provides for the treatment plans under consideration. For example, the

clinically prescribed dose level is lower than the optimum level by $\Delta\bar{D} = 8\text{-}14$ Gy (Tables 2 and 3). According to these findings, it is expected that a small increase in the dose prescription will slightly increase the complication rate but it will also be accompanied by a significant increase in the control rate. It can also be seen that in the qualitatively better treatment plans the curve of P_+ becomes higher and the width of the therapeutic window broadens, since the response curve of the CTV moves further away from those of the involved normal tissues. The width of the P_+ curve is a significant parameter since it is an index of how robust the treatment plan is against dose delivery and patient radiosensitivity uncertainties.

In this study, the importance of the $P - \bar{D}$ diagrams is illustrated. These diagrams provide important information by combining the radiobiological data of the organs involved with the dosimetric information of the delivered dose distribution in every clinical case. It would increase the flexibility and clinical application of the P_+ index if in its original definition the different terms related to the tumor control and normal tissue complication probabilities were accompanied by some weighting factors, which could be adjustable by the clinicians depending on the important of the different clinical endpoints used. By using the \bar{D} concept on the dose axis, the control and complication probabilities of the CTV and OARs can be examined individually. The major advantage is that the \bar{D}_B concept forces the total control probabilities of different plans to coincide and the comparison of the response curves becomes much simpler than when the mean target dose is used.

It is well known that the accuracy of the radiobiological models and the parameters characterizing the dose-response relation of the different tumors and healthy tissues is an important factor that also affected our results and conclusions. Moreover, we are aware of the fact that all the existing models are formulated based on certain assumptions or take under consideration specific only biological mechanisms. Additionally, the determination of the model variables describing the effective radiosensitivity of the tissues is influenced by the uncertainties occurred by the inaccuracies in the patient setup during radiotherapy, lack of knowledge of the inter-patient and intra-patient radiosensitivity and inconsistencies in treatment methodology.

It is worth of noticing that the OAR with the highest risk for complications is rectum in the case of CRT and bladder in the case of IMRT (Fig. 4). The statistical values presented in Tables 2-5 have been averaged over the results of the radiobiological treatment plan comparisons of each patient, separately. For this type of studies, this is the proper methodology rather than calculating the average CTV and OAR DVHs and then performing the radiobiological treatment plan comparisons based on these average DVHs. The reason for this difference is that the averaging process in the frame of DVHs is not compatible with the averaging process in the frame of dose-response curves. More specifically, the averaged tissue responses from the individual DVHs differ from the tissue responses that are calculated from the average DVHs. This is the reason of also showing the average dose-response curves in Figs. 4 and 5, whereas in Fig. 3, it is only the individual tissue DVHs that are presented. In Tables 2 and 3, it is shown that the variation of the results among the patients is fairly large.

In our implementation, we have retrieved the most of the tissue response parameters from recently published clinical studies that produced a significant reduction on these parameter confidence

intervals (for example, uncertainty of around 5% in the determination of D_{50}). As a result, there is some uncertainty appearing in the expected response of a tissue, which is in a clinically acceptable range.

However, both of the examined radiation modalities appear to have similar possibilities in producing highly conformal dose distributions. However, the superiority and possibilities of the two modalities would be illustrated in full scale if a radiobiological optimization could be performed before the treatment plan comparison [25]. We have shown that the P_+ and \bar{D} variables can be used for IMRT plan evaluation and provide great assistance in the choice of the most appropriate plan to be performed. Furthermore, the $(P - \bar{D})$ diagrams can be considered as the radiobiological version of the extensively used DVH diagrams. The importance of the proposed procedure is increased as more clinical data become available. The proposed evaluation procedure can be used in order to evaluate the treatment plan and the dose prescription. It is an excellent procedure to be followed in studies of dose escalation and response parameter determination.

In the future, target volumes could be reduced by both CT/MRI co-registration and dose painting using MR spectroscopy of choline and citrate in the prostate. These ongoing improvements and developments in radiotherapy treatment planning are leading to treatments which offer both better tumour volume coverage, and are minimising the risk of treatment-related complications. In time, these changes should allow the escalation in dose delivered to the tumour volume with the potential for increased cure rates [26].

Conclusions

The present study involved the evaluation of the effectiveness of conventional conformal, CRT and IMRT radiation modalities regarding the use of fused CT-MRI and CT alone images in treatment planning. Both physical and biological criteria were used in order to make the evaluation more complete. Our findings show that the use of fused CT-MRI images produce dose distributions, which lead on average to better expected treatment outcome compared to the use of CT images alone. This improvement decreases as we move from CRT techniques to IMRT treatments. Our study shows that the MLC-based IMRT radiation modality can produce treatment plans that deliver high uniform doses to the target with lower integral doses to healthy organs compared to CRT techniques.

The usage of radiobiological measures like P_+ and \bar{D} can improve the potential of achieving a good treatment plan. Radiobiological information provides assistance in evaluating the suitability of treatment plans and their association with the clinical result. The dose-response characteristics of the irradiated targets and normal tissues involved in a clinical case are a major part of such an analysis. The complementary relation of the radiobiological evaluation with the physical indices in analyzing a dose plan is indicated by their simultaneous presentation.

In order to achieve a better dose prescription basis for comparing treatment plans through evaluation of the biological outcome of the dose distributions, the \bar{D} biological dose can be used. The comparison of the different treatment plans of prostate cancer cases using the P_+ and \bar{D} variables

showed differences in the biological outcome of the plans. The findings of this study showed that although the clinical cases may be dosimetrically similar, the radiobiological indices of these cases can prove to be quite different. In these cases, the usage of $P_+ - \bar{\bar{D}}$ diagrams can prove to be a complimentary tool to the traditional dose based evaluation tools such as DVHs in order to compare and analyze the treatment plans.

It has been derived that IMRT can potentially limit the radiation doses applied to OARs. Nevertheless, the CTV expansion does not allow for much organ sparing when the target is adjacent to highly radiosensitive healthy organs. Although the 3D conformal radiotherapy technique that was applied is not characterized by a very high conformality, it is apparent that the better knowledge of the CTV extension improved considerably the produced dose distribution. The CTV is irradiated more homogeneously and rectum, which has the largest risk for complications, is spared better.

References

- [1] Chen L, Price RA Jr, Wang L, Li J, Qin L, McNeeley S, Ma CM, Freedman GM, Pollack A. MRI-based treatment planning for radiotherapy: dosimetric verification for prostate IMRT. *Int J Radiat Oncol Biol Phys* 2004;60: 636-47.
- [2] Jackson AS, Reinsberg SA, Sohaib SA, Charles-Edwards EM, Mangar SA, South CP, Leach MO, Dearnaley DP. Distortion-corrected T2 weighted MRI: a novel approach to prostate radiotherapy planning. *Br J Radiol* 2007;80: 926-33.
- [3] Villeirs GM, De Meerleer GO. Magnetic resonance imaging (MRI) anatomy of the prostate and application of MRI in radiotherapy planning. *Eur J Radiol* 2007;63: 361-8.
- [4] Villeirs GM, Van Vaerenbergh K, Vakaet L, Bral S, Claus F, De Neve WJ, Verstraete KL, De Meerleer GO. Interobserver delineation variation using CT versus combined CT + MRI in intensity-modulated radiotherapy for prostate cancer. *Strahlenther Onkol* 2005;181:424-30.
- [5] Rasch C, Barillot I, Remeijer P, Touw A, van Herk M, Lebesque JV. Definition of the prostate in CT and MRI: a multi-observer study. *Int J Radiat Oncol Biol Phys* 1999;43:57-66.
- [6] Debois M, Oyen R, Maes F, Verswijvel G, Gatti G, Bosmans H, Feron M, Bellon E, Kutcher G, Van Poppel H, Vanuytsel L. The contribution of magnetic resonance imaging to the three-dimensional treatment planning of localized prostate cancer. *Int J Radiat Oncol Biol Phys* 1999;45:857-65.
- [7] ICRU Report No. 62. Prescribing, recording and reporting photon beam therapy (A supplement to ICRU Report No. 50) International Commission on Radiation Units and Measurements; 1999.
- [8] Mavroidis P, Lind BK, Van Dijk J, Koedoeder K, De Neve W, De Wagter C, Planskoy B, Rosenwald JC, Proimos B, Kappas C, Danciu C, Benassi M, Chierego G, Brahme A. Comparison of conformal radiation therapy techniques within the dynamic radiotherapy project 'DYNARAD'. *Phys Med Biol* 2000;45:2459-81.
- [9] Mavroidis P, Lind BK, Brahme A. Biologically effective uniform dose ($\bar{\bar{D}}$) for specification, report and comparison of dose response relations and treatment plans. *Phys Med Biol* 2001;46:2607-30.
- [10] Källman P, Lind BK, Brahme A. An algorithm for maximizing the probability of complication free tumor control in radiation therapy. *Phys Med Biol* 1992;37: 871-90.
- [11] Brahme A. Which parameters of the dose distribution are best related to the radiation response of tumours and normal tissues. In: Proceedings of the Interregional Seminars for Europe, the Middle East and Africa Organized by the IAEA, Leuven, 1994;37-58.
- [12] Emami B, Lyman J, Brown A, Coia L, Goitein M, Munzenrider JE, Shank B, Solin LJ, Wesson AM. Tolerance of normal tissue to therapeutic irradiation. *Int J Radiat Oncol Biol Phys* 1991;21:109-22.
- [13] Ågren AK. Quantification of the response of heterogeneous tumors and organized normal tissues to fractionated radiotherapy. PhD Thesis, University of Stockholm, Sweden, 1995.

- [14] Mavroidis P, Laurell G, Kraepelien T, Fernberg JO, Lind BK, Brahme A. Determination and clinical verification of dose-response parameters for esophageal stricture from head and neck radiotherapy. *Acta Oncol* 2003;42: 865-81.
- [15] Mavroidis P, al-Abany M, Helgason AR, Ågren Cronqvist AK, Wersäll P, Theodorou K, Kappas C, Lind H, Lind BK, Steineck G, Brahme A. Dose-response relations for anal sphincter regarding faecal leakage and blood or phlegm in stools after radiotherapy for prostate cancer. *Strahlenther Onkol* 2005;181:293-306.
- [16] Ågren A-K, Brahme A, Turesson I. Optimization of uncomplicated control for head and neck tumors. *Int J Radiat Oncol Biol Phys* 1990; 19: 1077-85.
- [17] Källman P, Ågren AK, Brahme A. Tumor and normal tissue responses to fractionated non uniform dose delivery. *Int J Radiat Biol* 1992;62:249-62.
- [18] Jackson A, Ten Haken RK, Robertson JM, et al. Analysis of clinical complication data for radiation hepatitis using a parallel architecture model. *Int J Radiat Oncol Biol Phys* 1995; 31: 883-91.
- [19] Lind BK, Mavroidis P, Hyödynmaa S, Kappas C. Optimization of the dose level for a given treatment plan to maximize the complication free tumor cure. *Acta Oncol* 1999;38:787-98.
- [20] Brahme A. The need for accurate target and dose specifications in conventional and conformal radiation therapy – An introduction. *Acta Oncol* 1997;36:789-92.
- [21] Kölbl O, Richter S, Flentje M. Influence of treatment technique on dose-volume histogram and normal tissue complication probability for small bowel and bladder. *Strahlenther Onkol* 2000;176:105-11.
- [22] Parker CC, Damyanovich A, Haycocks T, Haider M, Bayley A, Catton CN. Magnetic resonance imaging in the radiation treatment planning of localized prostate cancer using intra-prostatic fiducial markers for computed tomography co-registration. *Radiother Oncol* 2003;66: 217-24.
- [23] Rosewall T, Kong V, Vesprini D, Catton C, Chung P, Ménard C, Bayley A. Prostate delineation using CT and MRI for radiotherapy patients with bilateral hip prostheses. *Radiother Oncol* 2009;90:325-30.
- [24] Steenbakkers RJ, Deurloo KE, Nowak PJ, Lebesque JV, van Herk M, Rasch CR. Reduction of dose delivered to the rectum and bulb of the penis using MRI delineation for radiotherapy of the prostate. *Int J Radiat Oncol Biol Phys* 2003;57:1269-79.
- [25] Ferreira BC, Svensson R, Löf J, Brahme A. The clinical value of non-coplanar photon beams in biologically optimized intensity modulated dose delivery on deep seated tumors. *Acta Oncol* 2003;42:852-64.
- [26] Beasley M, Driver D, Dobbs HJ. Complications of radiotherapy: improving the therapeutic index. *Cancer Imag* 2005;5:78-84.

Table 1

Summary of the model parameter values for the prostate cancer case. D_{50} is the 50% response dose, γ is the maximum normalized value of the dose-response gradient and s is the relative seriality, which characterizes the volume dependence of the organ.

Relative Seriality Model		Parameter Values		
Prostate cancer	D_{50} (Gy)	γ	s	α/β
CTV	80.0	4.0	—	10.0
Bladder	80.0	3.0	0.3	3.0
Rectum	80.0	2.2	0.7	3.0

Table 2

Summary of the dosimetric and radiobiological measures averaged over the 10 prostate cancer patients. The absolute values refer to the treatment plans, which are based on the CT images, whereas the differences express the deviations of the fused CT-MRI from the CT plans regarding the conventional conformal radiotherapy (CRT) technique.

Structures	<i>P</i> (%)	ΔP (%)	<i>D</i> _{mean}	ΔD _{mean}	<i>CV</i> (%)	ΔCV	$\bar{\bar{D}}$	$\Delta \bar{\bar{D}}$	<i>D</i> _{max}	ΔD _{max}	<i>D</i> _{min}	ΔD _{min}
CTV	26.5	0.0	75.5	0.0	0.5	-0.1	75.5	0.0	76.3	0.3	74.8	-0.1
Bladder	1.6	0.1	33.3	0.2	0.9	0.0	65.2	0.3	75.7	0.1	9.0	-0.1
Rectum	9.0	-1.7	47.1	-2.7	0.8	-0.1	67.1	-1.1	76.9	-0.1	3.8	-0.2
Dose prescription	Clinical						Optimum <i>P</i>₊					
Imaging modality	CT			CT – MRI			CT			CT – MRI		
<i>P</i> ₊ / ΔP ₊ (%)	15.9 ± 4.0 (9.9, 23.8)			1.6 ± 2.1 (-1.7, 4.9)			42.5 ± 10.4 (28.7, 62.6)			4.2 ± 6.0 (-5.7, 15.8)		
<i>P</i> _B / ΔP _B (%)	26.5 ± 1.6 (23.8, 29.6)			0.0 ± 0.7 (-1.1, 1.3)			80.0 ± 6.2 (68.3, 89.1)			0.6 ± 2.0 (-3.3, 3.2)		
<i>P</i> _I / ΔP _I (%)	10.5 ± 3.4 (5.5, 16.3)			-1.6 ± 1.9 (-4.3, 1.5)			37.4 ± 6.4 (26.5, 47.9)			-3.6 ± 4.8 (-12.8, 3.0)		
$\bar{\bar{D}}$ _B / $\Delta \bar{\bar{D}}$ _B (Gy)	75.5 ± 0.3 (75.0, 76.0)			0.0 ± 0.1 (-0.2, 0.2)			86.4 ± 2.1 (83.0, 90.0)			0.3 ± 0.8 (-1.0, 2.0)		

Table 3

Summary of the dosimetric and radiobiological measures averaged over the 10 prostate cancer patients. The absolute values refer to the treatment plans, which are based on the CT images, whereas the differences express the deviations of the fused CT-MRI from the CT plans regarding the intensity modulated radiotherapy (IMRT) technique.

Structures	P (%)	ΔP (%)	D_{mean}	ΔD_{mean}	CV (%)	ΔCV	$\bar{\bar{D}}$	$\Delta \bar{\bar{D}}$	D_{max}	ΔD_{max}	D_{min}	ΔD_{min}
CTV	57.1	1.5	81.0	0.2	0.7	0.0	80.8	0.3	84.4	-0.1	77.7	0.7
Bladder	3.1	0.4	29.1	0.4	0.4	0.0	63.0	1.0	76.1	0.4	6.7	-0.2
Rectum	1.6	0.2	34.0	-1.9	0.4	0.0	58.8	-1.5	71.5	-2.7	7.1	-2.4
Dose prescription	Clinical						Optimum P_+					
Imaging modality	CT			CT – MRI			CT			CT – MRI		
$P_+ / \Delta P_+$ (%)	52.5 ± 8.1 (37.8, 63.4)			0.9 ± 10.6 (-22.3, 13.6)			74.7 ± 13.0 (58.7, 90.7)			0.0 ± 10.5 (-20.5, 13.2)		
$P_B / \Delta P_B$ (%)	57.1 ± 8.1 (38.4, 65.5)			1.5 ± 9.9 (-15.1, 16.9)			90.0 ± 5.8 (82.1, 96.6)			0.2 ± 3.5 (-7.8, 3.8)		
$P_I / \Delta P_I$ (%)	4.7 ± 3.7 (0.2, 10.3)			0.5 ± 3.3 (-4.0, 7.2)			15.3 ± 7.4 (4.4, 23.4)			0.1 ± 7.4 (-9.4, 16.5)		
$\bar{\bar{D}}_B / \Delta \bar{\bar{D}}_B$ (Gy)	80.8 ± 1.5 (77.5, 82.4)			0.3 ± 1.9 (-2.7, 2.9)			91.5 ± 3.9 (86.9, 96.9)			0.6 ± 3.3 (-7.0, 6.0)		

Table 4

Summary of the dosimetric and radiobiological measures averaged over the 10 prostate cancer patients. The values of the differences express the deviations of the fused CT-MRI from the CT plans regarding the conventional conformal radiotherapy (CRT) technique.

TISSUE	ΔP (%)	$\Delta \bar{D}$ (Gy)	$\Delta \bar{D}$ (Gy)	ΔCV	ΔD_{\max}	ΔD_{\min}
CTV	0.0	0.0	0.0	0.0	0.1	0.0
Bladder	0.0	0.0	0.0	0.0	0.0	0.0
Rectum	0.0	0.0	0.0	-0.1	0.0	0.0
Dose Prescription	Clinical			Optimum P_+		
ΔP_+ (%)	0.0 ± 0.4 (-1.0, 0.4)			0.0 ± 0.2 (-0.5, 0.2)		
ΔP_B (%)	0.0 ± 0.4 (-1.0, 0.4)			0.0 ± 0.0 (0.0, 0.0)		
ΔP_I (%)	0.0 ± 0.0 (0.0, 0.0)			0.0 ± 0.2 (-0.2, 0.5)		
$\Delta \bar{D}_B$ (Gy)	0.0 ± 0.1 (-0.2, 0.1)			0.0 ± 0.0 (0.0, 0.0)		

Table 5

Summary of the dosimetric and radiobiological measures averaged over the 10 prostate cancer patients. The values of the differences express the deviations of the fused CT-MRI from the CT plans regarding the intensity modulated radiotherapy (IMRT) technique.

TISSUE	ΔP (%)	$\Delta \bar{D}$ (Gy)	$\Delta \bar{D}$ (Gy)	ΔCV	ΔD_{\max}	ΔD_{\min}
CTV	-2.1	-0.4	-0.3	0.1	-0.2	-0.7
Bladder	0.0	0.0	0.0	0.0	0.0	0.0
Rectum	0.0	0.0	0.0	0.0	0.0	0.0
Dose Prescription	Clinical			Optimum P_+		
ΔP_+ (%)	-2.1 ± 7.8 (-15.2, 8.6)			-0.4 ± 3.5 (-7.8, 5.5)		
ΔP_B (%)	-2.1 ± 7.8 (-15.2, 8.6)			-0.5 ± 0.7 (-2.0, 0.1)		
ΔP_I (%)	0.0 ± 0.0 (0.0, 0.0)			-0.2 ± 3.1 (-5.7, 6.4)		
$\Delta \bar{D}_B$ (Gy)	-0.4 ± 1.5 (-2.7, 1.9)			-0.4 ± 0.4 (-1.0, 0.0)		

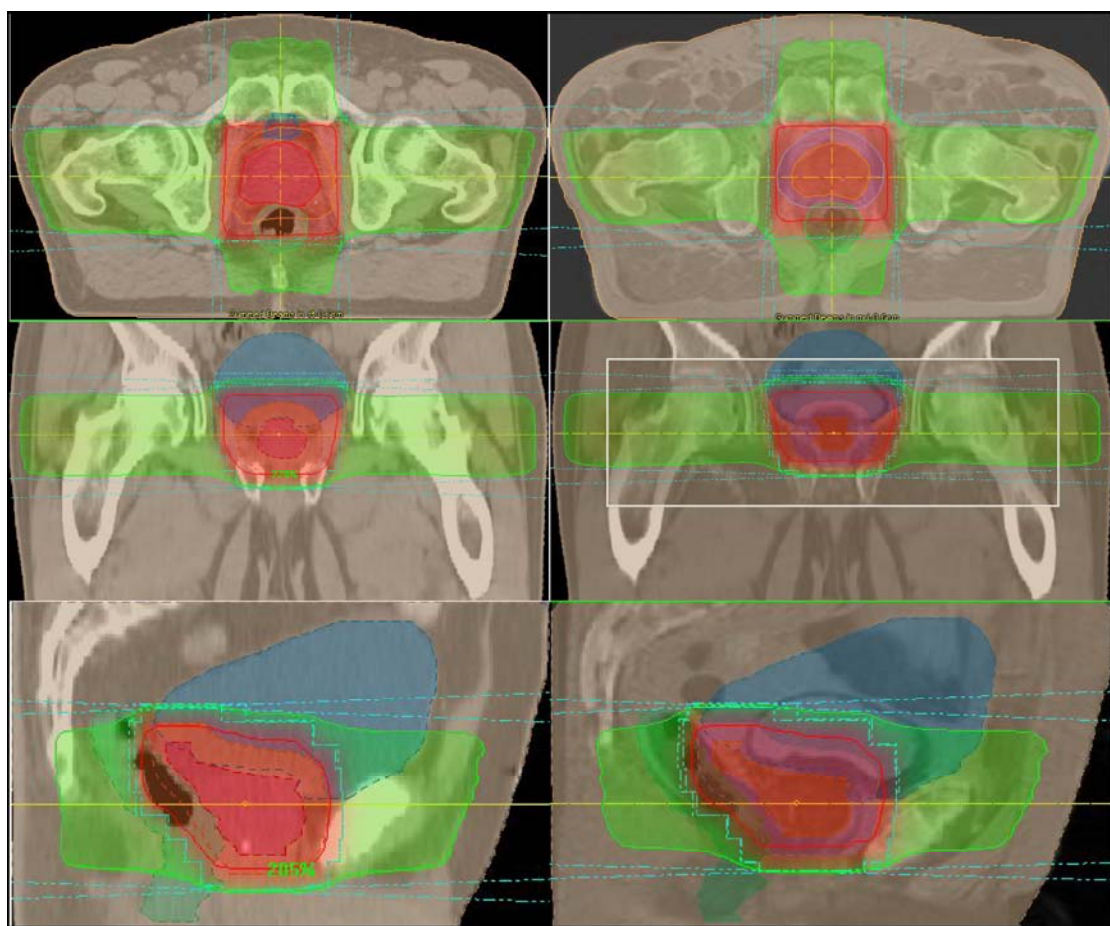


Fig. 1. The reference CT (left) and MRI (right) slices of a prostate cancer patient is shown for the 3D-CRT treatment plans in the transverse and coronal and sagittal planes. The delineations of the anatomical structures involved were performed based on the CT and MRI images and they are illustrated together with the dose distributions delivered to the patient.

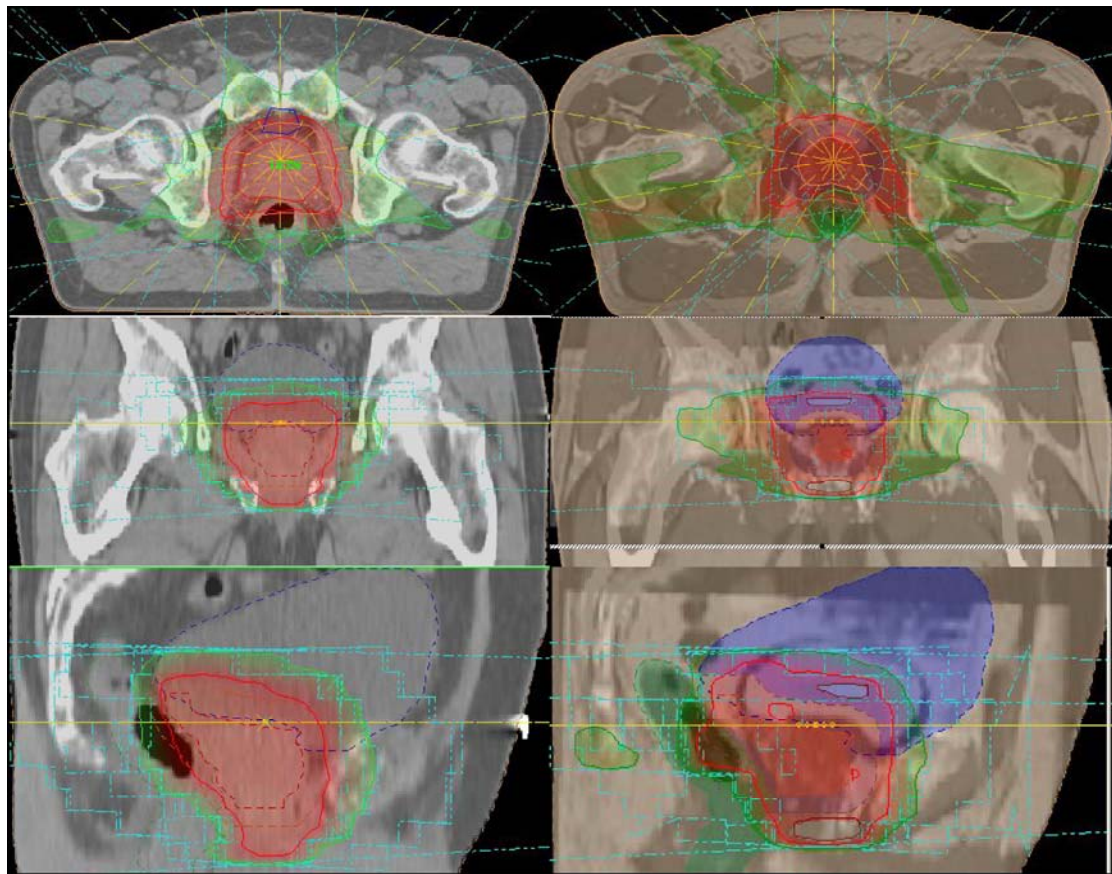


Fig. 2. The reference CT (left) and MRI (right) slices of a prostate cancer patient is shown for the MLC-based IMRT treatment plans in the transverse and coronal planes. The delineations of the anatomical structures involved were performed based on the CT and MRI images and they are illustrated together with the dose distributions delivered to the patient.

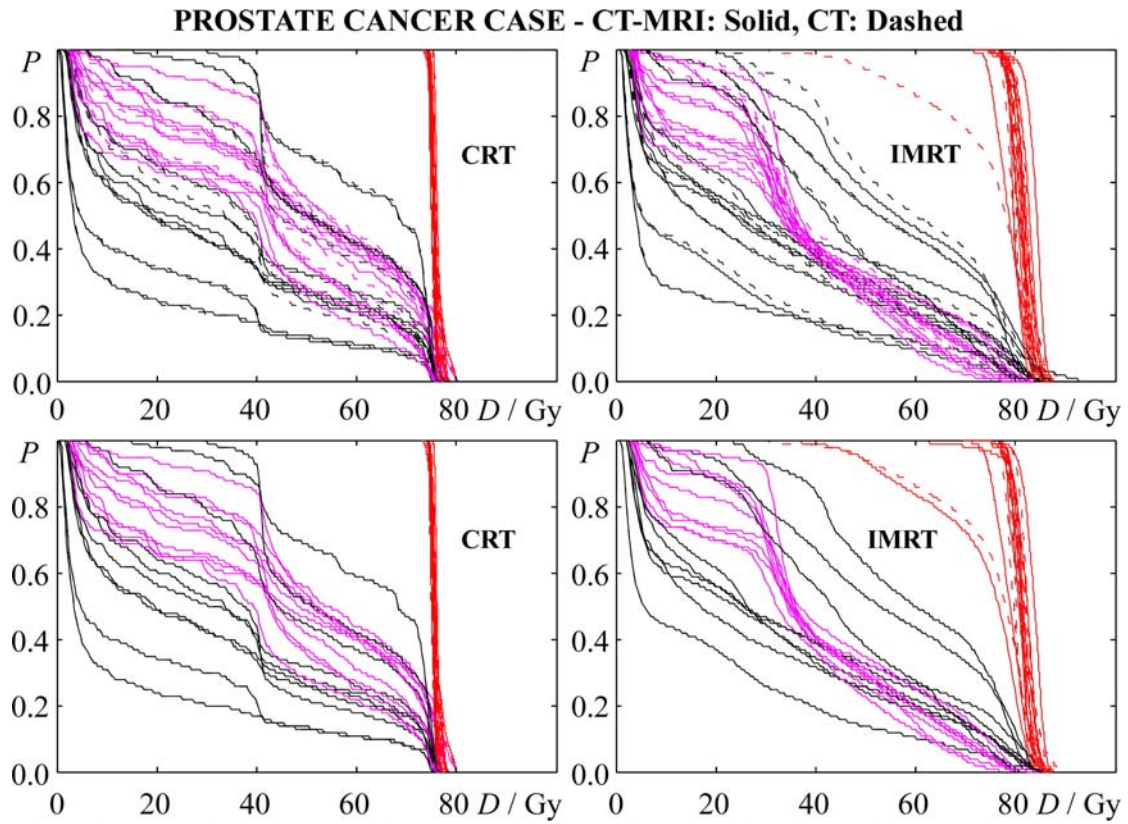


Fig. 3. In the upper diagrams, the DVHs of the CTV (red), bladder (black) and rectum (pink) are presented for the CRT and IMRT treatment plans, which were optimized based on the CT and fused CT-MRI images separately. In the lower diagrams, the DVHs of the different tissues are presented for the CRT and IMRT treatment plans, which were optimized based on the CT images. In these diagrams the solid curves represent the DVHs of the different tissues when the fused CT-MRI delineations were used on the CT-based treatment plans.

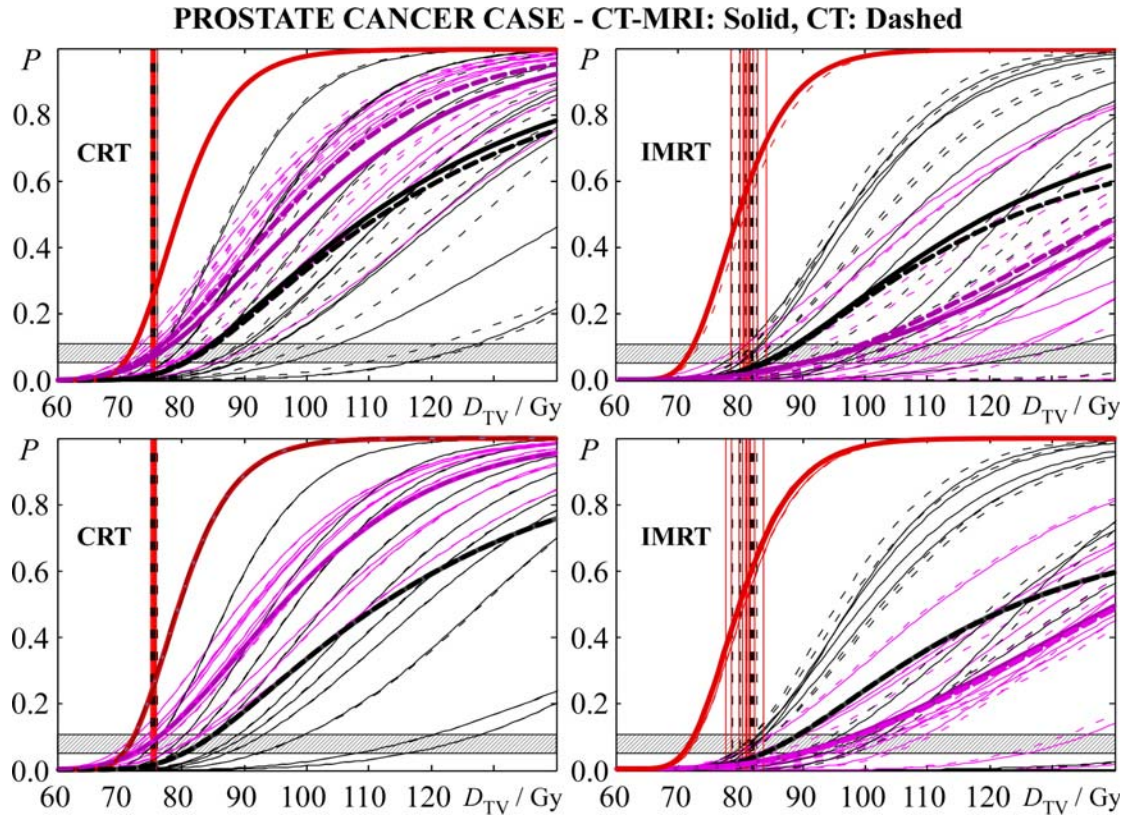


Fig. 4. In the upper diagrams, the dose-response curves of the CTV (red), bladder (black) and rectum (pink) are presented for the CRT and IMRT treatment plans, which were optimized based on the CT and fused CT-MRI images separately. In the lower diagrams, the dose-response curves of the different tissues are presented for the CRT and IMRT treatment plans, which were optimized based on the CT images. In these diagrams the solid curves represent the dose-response curves of the different tissues when the fused CT-MRI delineations were used on the CT-based treatment plans.

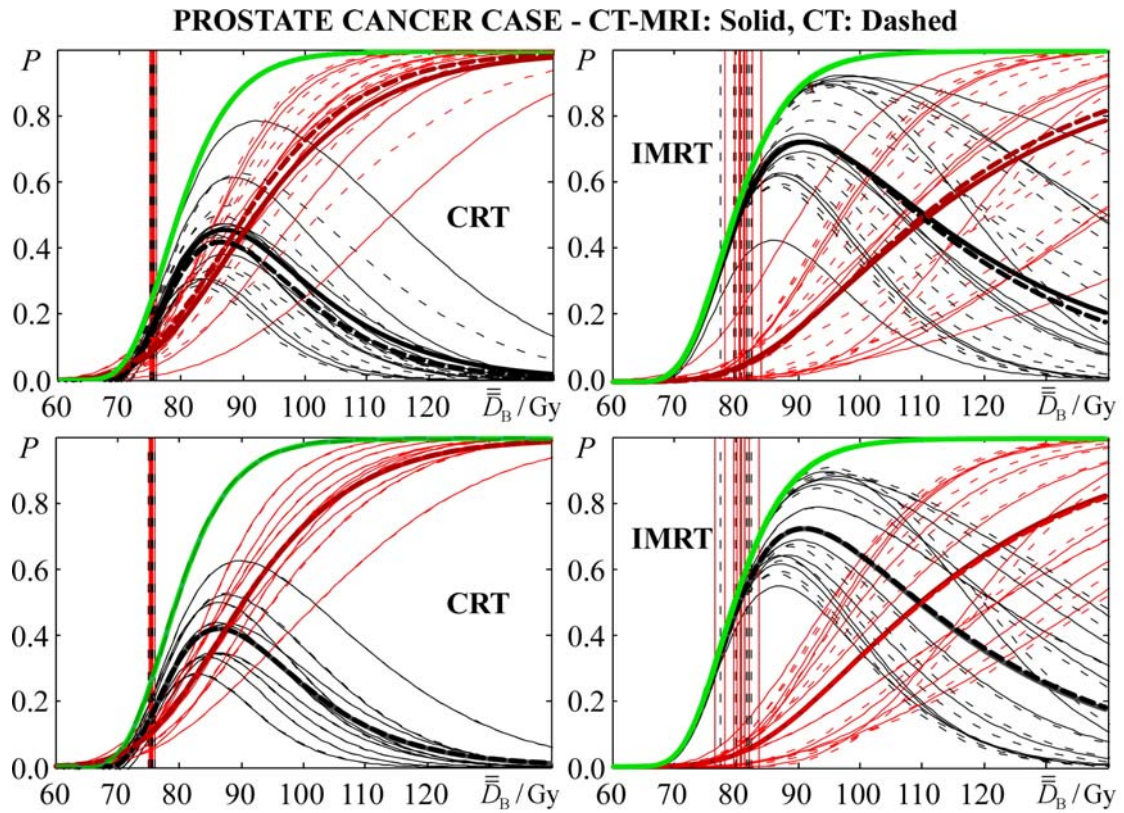


Fig. 5. In the upper diagrams, the curves of the total control probability, P_B (green), total complication probability, P_1 (red) and complication-free tumor control probability, P_+ (black) are presented for the CRT and IMRT treatment plans, which were optimized based on the CT and fused CT-MRI images separately. In the lower diagrams, the curves of the P_B , P_1 and P_+ are presented for the CRT and IMRT treatment plans, which were optimized based on the CT images. In these diagrams the solid curves represent the dose-response curves when the fused CT-MRI delineations were used on the CT-based treatment plans.